Path Integral Monte Carlo and Density Functional Molecular Dynamics Simulations of Warm, Dense Neon

K. P. Driver[1,*] and B. Militzer[1,2]

[1]*Department of Earth and Planetary Science, University of California, Berkeley, California 94720, USA*
[2]*Department of Astronomy, University of California, Berkeley, California 94720, USA*

(Dated: June 18, 2014)

All-electron path integral Monte Carlo (PIMC) and density functional theory molecular dynamics (DFT-MD) allow for a consistent first-principles investigation of hot, dense neon plasmas in the density-temperature range of 1–15 g cm^{-3} and 10^4–10^8 K. DFT-MD data at low temperatures combined with PIMC data at higher temperatures provides a coherent equation of state with a region of overlap in which the two methods cross-validate each other. PIMC and DFT-MD and pressures, internal energies, and pair-correlation functions are shown to agree at temperatures near 1×10^6 K. At higher temperatures, DFT-MD becomes intractable because of too many partially occupied bands, while at lower temperatures, PIMC is intractable because of approximations to fermion nodes. We find neon remains an insulator even for the highest density-temperature conditions studied with DFT-MD here. The computed shock Hugoniot curves show an increase in compression as the first and second shells are ionized.

PACS numbers: 62.50.-p,31.15.A-,61.20.Ja,64.30.-t

I. INTRODUCTION

Theoretical prediction of thermodynamic properties of warm, dense matter[1] (WDM) plays an important role in furthering our understanding of a large variety of high energy density physics applications, including inertial confined plasmas[2,3], shock[4], astrophysical processes[5,6], stellar and planetary interiors[7], and supernovae[8]. In order to understand the thermodynamic properties of these physical processes, one must develop accurate methods to predict the equation of state (EOS) of plasmas. The development of a comprehensive first-principles methodology for this purpose remains a great challenge.

The difficulty in treating the physics of the WDM regieme is that plasmas partially ionized such that the electron-ion Coulomb interaction is comparable in magnitude to the kinetic energy. Effects of bonding, ionization, exchange-correlation, and quantum degeneracy all contribute significantly to the total energy[1]. A number of analytic and numerical methods, employing various levels of classical and quantum physics, have been developed to study plasamas in various regimes[9,10], but it is difficult to link them together in a thermodynamically consistent way.

In an effort to develop a comprehensive first-principles treatment of WDM, we have been working on the development of a combined aproach using density functional theory molecular dynamics (DFT-MD) at low temperatures and path integral Monte Carlo at high temperatures[11,12]. Prior to our work, PIMC had been applied only to the lighest two elements, hydrogen[13] and helium[11]. We showed that all-electron PIMC with free-particle nodes is a feasible route to study even heavier elements, computing EOSs for both water and carbon plasmas[12]. In the current work, we aim to press the limits of our techique and show that it is capable of producing an EOS for elements as heavy as neon.

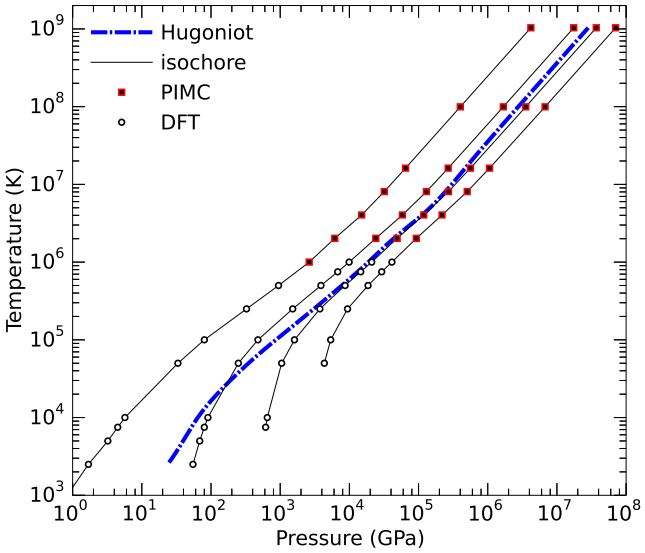

FIG. 1: (color online) Temperature-pressure conditions for the PIMC and DFT-MD calculations along four isochores corresponding to the densities of 0.8949, 3.7283, 7.8959, and 15.0255 g cm^{-3}. The dash-dotted line shows the Hugoniot curve for an initial density of $\rho_0 = 1.5070$ g cm^{-3}.

Neon is itsef an interesting an important material in the universe, as it is the fifth most abundant element after H, He, O, and C. During nucleosynthesis, neon is created during the carbon-burning process. As an inert gas, neon is highly volitile, and, therefore, easily depleted from atmospheres of even giant gas planets such as Jupiter[14]. Due to stellar and planetary interest in neon, a number of studies have been done for various hot, dense conditions[15–17].

In this paper, we aim to produce a comprehen-

sive, first-principles EOS for neon that covers a large temperature-density space (0.8949–15.0255 $\mathrm{g\,cm^{-3}}$ and 10^4–10^8 K). In Section II, we discuss the details of PIMC and DFT-MD methods used for our calculations. In Section III, we provide the EOS of over a wide temperature-density range and show that both PIMC and DFT-MD agree near 1×10^6 K, where both methods are feasible. In section IV, we characterize the structure of the plasma by looking at various pair-correlation functions of electrons and nuclei. In section V, we show the electronic density of states for our DFT-MD calculations at the most extreme conditions. We find neon is still an insulator at 1×10^6 K and 15.0255 $\mathrm{g\,cm^{-3}}$. Finally, in section VI, we discuss predictions for the for the shock Hugoniot curves.

II. METHODS

A rigorous discussion of PIMC[18] and DFT methods[19] and the details of our specific PIMC implementation have been reported previously[11]. In this section, we focus only on details that are important for specific neon simulations.

PIMC is a first-principles method for studying materials at high temperature where properties of materials are dominated by excited states. The thermal density matrix, which is efficiently computed within Feynman's path integral formalism, is the natural operator to use for computing of high-temperature observables. The PIMC method stochastically solves the full finite-temperature quantum many-body problem by treating electrons and nuclei on an equal footing. In contrast to DFT, PIMC efficiency increases with temperature as particles become more classical and fewer time slices are needed to describe quantum mechanical many-body correlations, scaling inversely with temperature.

PIMC uses a fixed nodal surface to avoid the fermion sign problem. Thus far, all PIMC implementations have employed a free-particle nodal structure, which is expected to be a good approximation for systems that are close to a fully ionized state. However, reliable results at surprising low temperatures have been obtained for hydrogen[13], as well as carbon and water[12]. These results showed that free particle nodes are sufficient for a filled 1s states and 2s states that are sufficiently ionized. The use of free particle nodes as well as the lack of a non-local pseudopotential formulation[20] have limited its application to heavier elements.

For our PIMC simulations, the Coulomb interaction is incorporated via pair density matrices derived from the eigenstates of the two-body Coulomb problem. A sufficiently small time step is determined by converging total energy as a function of time step until the energy changes less than 0.2%. We use a time step of $1/256$ $\mathrm{Ha^{-1}}$ for temperatures below 4×10^6 K and, for higher temperatures, the time step decreases as $1/T$ while keeping at least five time slices in the path integral. In order to minimize finite size errors, the total energy is converged to better than 0.2% for both 8- and 24- atom simple cubic simulation cells.

The framework of DFT provides an exact mapping of the many body problem onto a single particle problem, assuming an approximate exchange-correlation (XC) functional is known. For all but the simplest model systems, approximate XC functionals most widely used have been constructed based on data from zero temperature quantum Monte Carlo calculations of the electron gas[21]. In the WDM regime, where temperatures are at or above the Fermi temperature, there is no expectation for an XC functional to provide accuracte description of the electronic physics. However, in previous PIMC and DFT-MD work on the electron gas[22], carbon[12], and water[12], it was shown that DFT functionals are are surprisingly accurate at very high temperatures.

Finite-temperature DFT uses a Fermi-Dirac function to allow for thermal occupation of single-particle electronic states[23], but requires an increasing number of bands with temperature, crippling its efficiency at extreme temperatures. In addition, typically pseudopotentials replace the core electrons in each atom. It is possible the pseudopotential approximation may break down and should be compared with all-electron calculations, particularly as electrons are thermally excited out of the core. Orbital-free density functional methods aim to overcome such thermal band limitations, but several challenges remain to be solved[24].

The DFT-MD simulations were performed with the Vienna *Ab initio* Simulation Package (VASP)[25] using the projector augmented-wave (PAW) method[26]. MD uses a NVT ensemble regulated with a Nosé-Hoover thermostat. Exchange-correlation effects are described using the Perdew-Burke-Ernzerhof[27] generalized gradient approximation. Electronic wave functions are expanded in a plane-wave basis with a energy cutoff of at least 1000 eV in order to converge total energy to chemical accuracy. Size convergence tests up to a 24-atom simulation cell at temperatures of 10,000 K and above indicate that total energies are converged to better than 2% in a 8-atom simple cubic cell. We find, at temperatures above 250,000 K, 8-atom cell results are sufficient since the kinetic energy far out weighs the interaction energy as such high temperatures. The number of bands in each calculation is selected such that thermal occupation is converged to better than 10^{-4}, which requires up to 9,000 bands in the highest temperature cases corresponding with the lowest density. All simulations are performed at the gamma-point of the Brillouin zone, which is sufficient for high temperature fluids, converging total energy to 0.01%

III. EQUATION OF STATE RESULTS

In this section, we report our EOS results for four densities of 0.8949, 3.7283, 7.8959, and 15.0255 $\mathrm{g\,cm^{-3}}$ and for a temperature range of 10^4-10^9 K. The four isochores are shown in Figure 1.

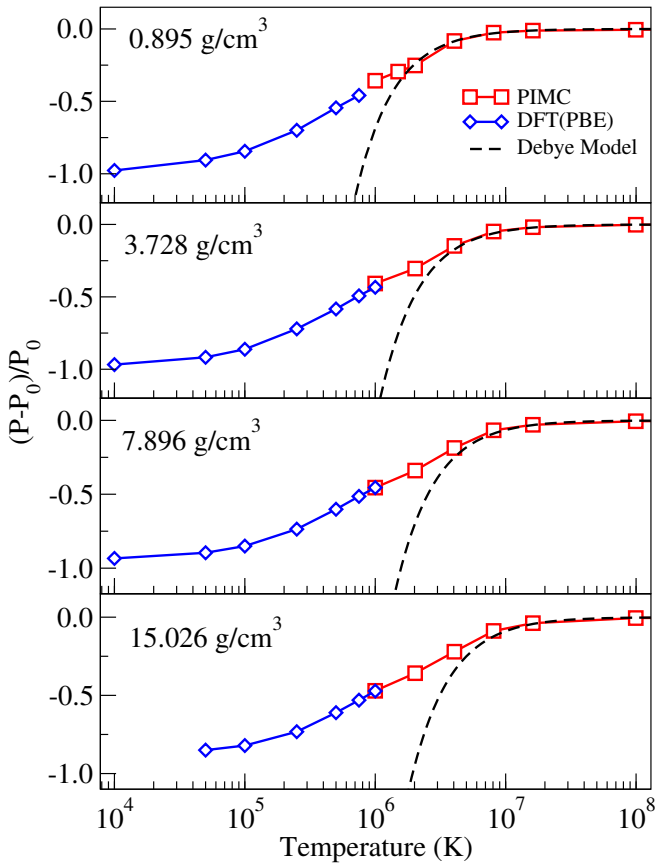

FIG. 2: (color online) Comparison of excess pressure relative to the ideal Fermi gas plotted as a function of temperature for neon.

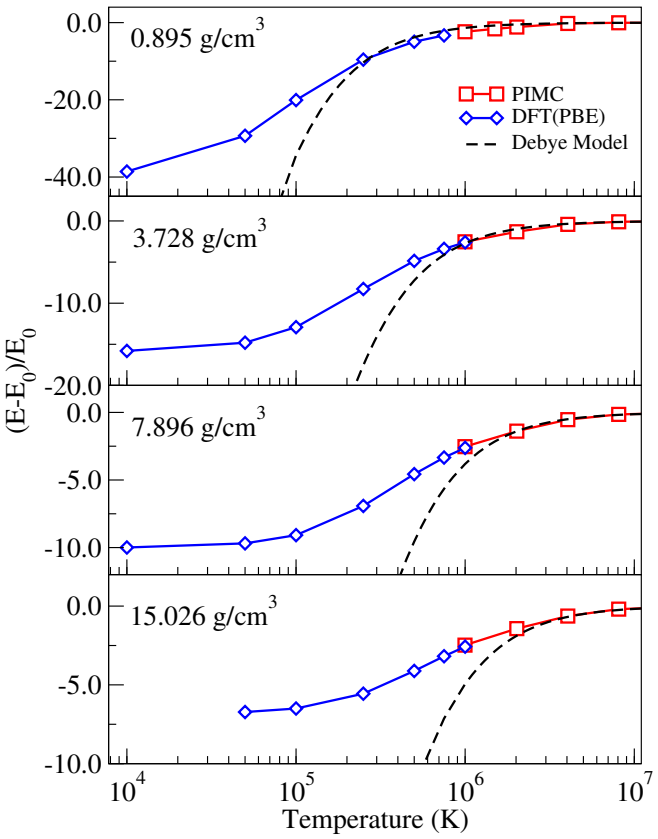

FIG. 3: (color online) Comparison of excess internal energies relative to the ideal Fermi gas plotted as a function of temperature for neon.

Figure 2 compares pressures obtained for neon from PIMC and DFT-MD simulations and from the analytical Debye-Hückel plasma model[28]. Pressures, P, are plotted relative to a fully ionized Fermi gas of electrons and ions with pressure, P_0, in order to compare only the excess pressure contributions that result from particle interactions. DFT-MD excess pressures agree with PIMC to better than 0.05% at 10^6 K for the largest three densities. For the lowest density, we were unable to obtain converged DFT result at 10^6 K, and free-particle nodes in PIMC start to break down at that point. Nonetheless, the excellent agreement near 10^6 K at all higher densities allows for cross-validation between DFT and PIMC, which implies the zero temperature DFT exchange-correlation potential remains valid at high temperatures and that the free-particle nodal approximation is valid in PIMC when atoms are partially and fully ionized. For the smallest density, we find the 2s state is 15% occupided when free particle nodes start to break down, while for the largest density, the 2s state is only 50% occupied at the breaking point. The two methods have comparable computational cost in the overlap region, but DFT computational cost starts to become prohibitive beyond 7.5×10^5 K, and free particle nodes break down below 10^6 K for all densities.

Figure 3 compares internal energies, E, plotted relative to the internal energy of a fully ionized Fermi gas, E_0. PIMC and DFT-MD results for excess internal energy agree to better than 0.04% at 10^6 K for the largest three densities. The DFT-MD and PIMC methods together form a coherent equation of state over all temperatures ranging to the weakly interacting plasma limit. PIMC extends the equations of state to the weakly interacting plasma limit at high temperatures, in agreement with the Debye-Hückel model[28].

Table I provides the densities, temperatures, pressures and energies used to construct our EOSs. The DFT-MD energies have been shifted by 128.8661280 Ha/atom in order to shift the the PAW pseudpotential reference energy back to the absolute atomic energy. The shift was calculated by performing an all electron atomic calculation in the OPIUM Code[29] and a corresponding isolated atom calculation in VASP.

TABLE I: EOS table with pressures and internal energies per atom. The numbers in parentheses indicates the statistical uncertainties of the DFT-MD and PIMC simulations.

ρ (g cm^{-3})	T (K)	P (GPa)	E (Ha/atom)
0.8948[a]	1034730000	4196329(484)	54055(6)
0.8948[a]	99497670	401383(260)	5170(3)
0.8948[a]	16167700	64842(37)	826.1(5)
0.8948[a]	8083850	31972(14)	400.5(3)
0.8948[a]	4041920	15045(7)	164.5(2)
0.8948[a]	2020960	6150(18)	-15.7(3)
0.8948[a]	1497010	4305(13)	-49.0(2)
0.8948[a]	998004	2625(25)	-72.2(3)
0.8948[b]	750000	fix-16atom	fix
0.8948[b]	500000	fix-16atom	fix
0.8948[b]	250000	326.1(4)	-120.226(1)
0.8948[b]	100000	80.1(2)	-126.792(1)
0.8948[b]	50000	33.2(8)	-128.204(1)
0.8948[b]	10000	5.70(5)	-128.816(1)
0.8948[b]	7500	4.48(4)	-128.829(1)
0.8948[b]	5000	3.23(2)	-128.842(1)
0.8948[b]	2500	1.69(2)	-128.856(1)
0.8948[b]	1000	0.83(2)	-128.864(1)
3.7283[a]	1034730000	17481714(2218)	54050(7)
3.7283[a]	99497670	1678235(1064)	5181(3)
3.7283[a]	16167700	268122(157)	813.3(5)
3.7283[a]	8083850	130114(63)	379.5(3)
3.7283[a]	4041920	58450(28)	123.7(1)
3.7283[a]	2020960	24061(78)	-33.0(2)
3.7283[b]	1000000	9923(4)	-86.770(4)
3.7283[b]	750000	6786(4)	-99.176(7)
3.7283[b]	500000	3882(4)	-111.229(5)
3.7283[b]	250000	1516(4)	-122.180(6)
3.7283[b]	100000	477(2)	-127.211(4)
3.7283[b]	50000	248(4)	-128.280(5)
3.7283[b]	10000	90.2(2)	-128.767(1)
3.7283[b]	7500	80.0(2)	-128.786(1)
3.7283[b]	5000	68.6(1)	-128.804(1)
3.7283[b]	2500	54.9(1)	-128.825(1)
7.8959[a]	1034730000	37020409(4549)	54042(7)
7.8959[a]	99497670	3540121(2430)	5155(4)
7.8959[a]	16167700	561943(312)	798.5(5)
7.8959[a]	8083850	270886(130)	362.6(3)
7.8959[a]	4041920	118753(49)	99.5(1)
7.8959[a]	2020960	49057(164)	-41.8(2)
7.8959[b]	1000000	21019(31)	-91.23(2)
7.8959[b]	750000	14588(36)	-102.47(2)
7.8959[b]	500000	8675(37)	-113.23(1)
7.8959[b]	250000	3750(18)	-122.78(1)
7.8959[b]	100000	1608(9)	-127.125(7)
7.8959[b]	50000	1050(8)	-128.105(6)
7.8959[b]	10000	650.8(5)	-128.576(1)
7.8959[b]	7500	616.1(7)	-128.576(1)
15.0255[a]	1034730000	70454931(8274)	432356(51)
15.0255[a]	99497670	6738033(4770)	5152(4)
15.0255[a]	16167700	1061043(1255)	785(1)
15.0255[a]	8083850	505320(302)	342.8(3)
15.0255[a]	4041920	218379(136)	79.1(1)
15.0255[a]	2020960	92899(342)	-47.6(2)

TABLE I. (Continued.)

ρ (g cm^{-3})	T (K)	P (GPa)	E (Ha/atom)
15.0255[b]	1000000	41193(82)	-94.34(4)
15.0255[b]	750000	29324(37)	-104.66(2)
15.0255[b]	500000	18607(35)	-114.22(1)
15.0255[b]	250000	9400(17)	-122.70(1)
15.0255[b]	100000	5370(23)	-126.55(1)
15.0255[b]	50000	4346(20)	-127.44(1)

[a] PIMC
[b] DFT-MD

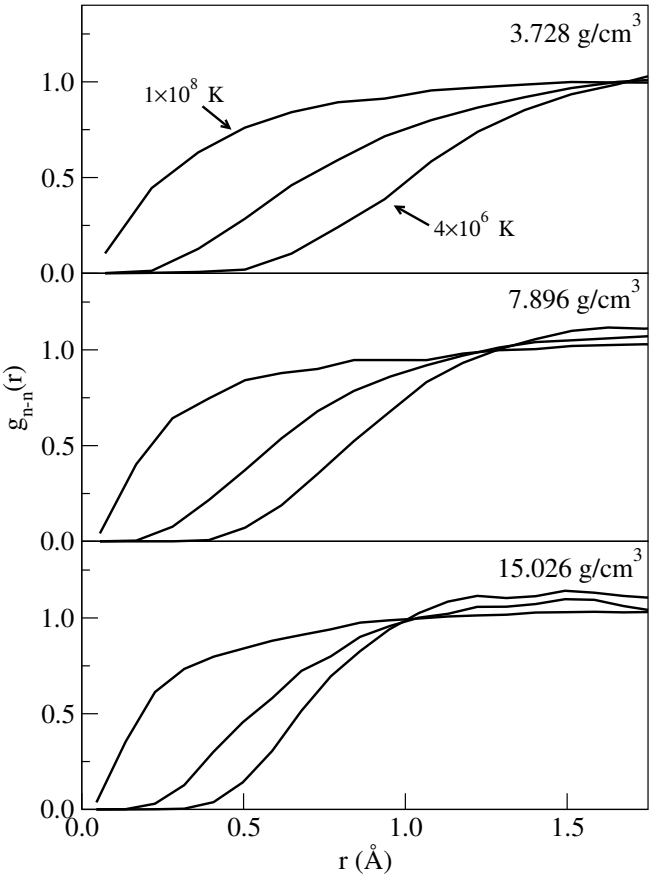

FIG. 4: (color online) Nuclear pair-correlation functions for neon from PIMC at temperatures of 4×10^6, 1.6×10^7, and 1×10^8 K for each density.

IV. PAIR-CORRELATION FUNCTIONS

In this section, we study the structure of neon plasmas. Pair-correlation functions[30] between the various particles are analyzed as a function of temperature and density. The data gives insight into details of the temperature-driven ionization process.

Figure 4 shows nuclear pair-correlation functions computed with PIMC. At low temperature, the atoms are kept farthest apart as atoms are repelled by Pauli re-

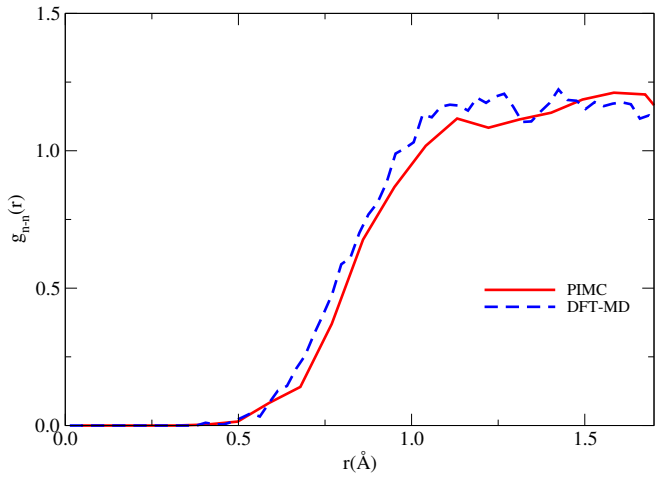

FIG. 5: (color online) Comparison of PIMC and DFT nuclear pair-correlation functions for neon at 1×10^6 K.

pulsion amongst the bound electrons as well as by their Coulomb interaction. As temperature increases, the nuclei gain kinetic energy leading to stronger collisions, and atoms become more ionized, gradually minimizing effects of Pauli repulsion. At the highest temperature, the system approaches the Debye-Hückel limit, behaving like a correlated system of screened Coulomb charges. The $g(r)$ functions depend only weakly on the density. Still at high density, the chance of finding two nuclei at close range is slightly increrased.

Figure 5 compares the nuclear pair-correlation functions of PIMC and DFT at a temperature of $1{\times}10^6$ K. These $g(r)$ curves verify that PIMC and DFT predict consistent structural properties in addition to the agreement in the equation of state.

Figure 6 shows $N(r)$, the integral of the pair correlations, that represent the average number of electrons within a sphere of radias r around a given nucleus. This number decreases with increasing temperature as atoms become ionized and electrons become unbound. At low density, the 1s core state is fully occupied at $1{\times}10^6$ K, as it agrees with the isolated 1s core state. Ionization of the 1s occurs over the temperature interval from 1 to 8 $\times 10^6$ K. At high density, the 1s core state is still fully occupied at temperatures up to $2{\times}10^6$ K, indicating ionization fraction still decreases with density and is not pressure-driven process as would expected if neon were close to metallization. In the next section, we demonstrate the neon remains an insulator for all densities under consideration.

Figure 7 shows nucleus-electron pair correlations as a function of temperature and density. At low temperature and high density, we find more electrons near the nuclei, reflecting a lower ionization fraction. At higher temperatures, electrons are thermally excited and gradually become unbound, decreasing their correlation with the nuclei. As the density is increased, the electrons are

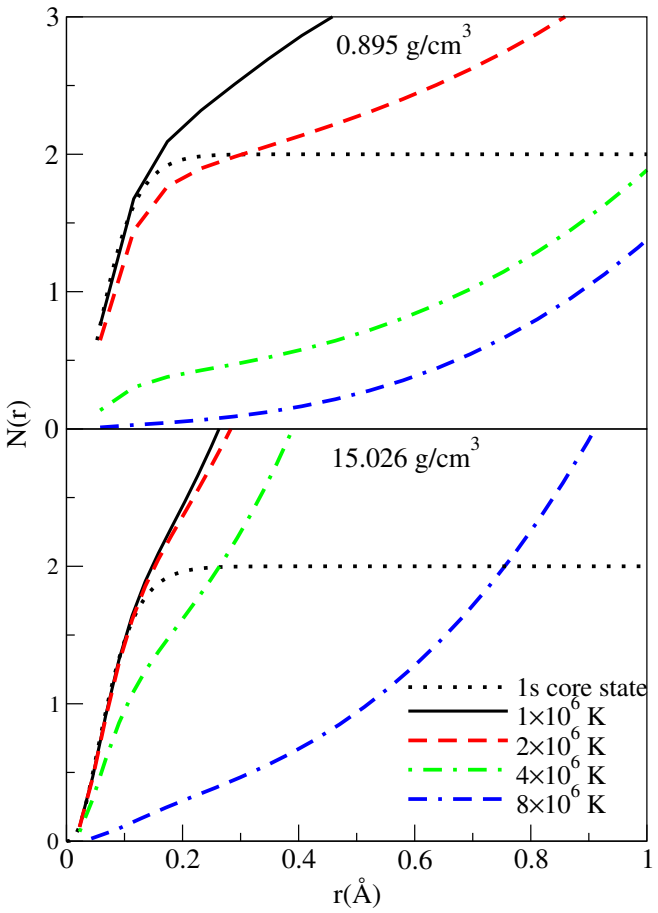

FIG. 6: (color online) Number of electrons contained in a sphere of radius, r, around a neon nucleus.

more likely to reside near the nuclei confirming the absence of any pressure-drive ionization seen in Fig. 6.

Figure 8 shows electron-electon pair-correlations with their spins opposite. The function is multiplied by the particle density ρ, so that the integral under the curves is related to the number of electrons **fix**. The electrons are most highly correlated for low temperatures since electrons are most strongly bound to the nuclei in those cases. As temperature increases, electrons are thermally excited, decreasing the correlation. Higher densities increase correlation at short distances, consistent with a lower ionization fraction.

Figure 9 shows electron-electon pair-correlations with their spins parallel. The shape of those functions are controlled by two effects. Different elelctrons with parallel spin are bound to a single nucleus, which lead to a positive correlation at intermediate distances. For short separations, Pauli exclusion takes over and thus all those function decay to zero for small r.

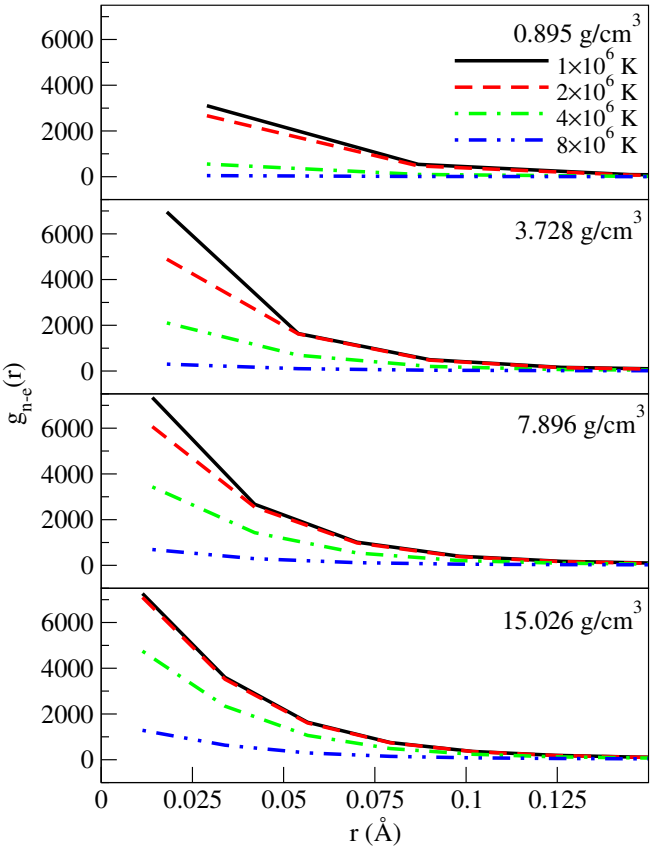

FIG. 7: (color online) The electron-nucleus pair-correlation functions calculated with PIMC.

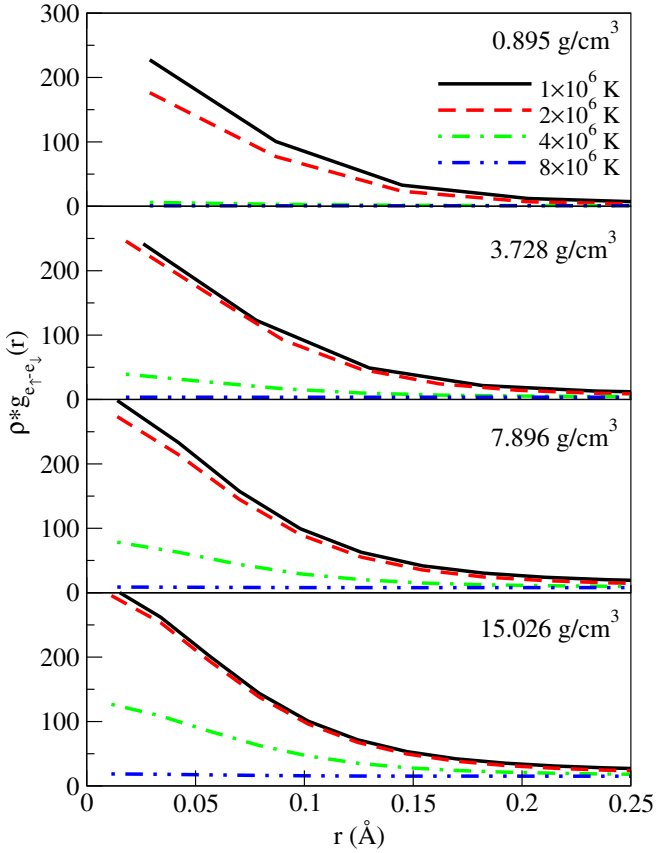

FIG. 8: (color online) The electron-electron pair-correlation functions for electrons with opposite spins calculated with PIMC.

V. ELECTRONIC DENSITY OF STATES

In this section, we briefly examine whether the effects of high temperature and density can introduce closure of the electronic band gap in fluid neon. Solid neon is the material with the highest metallization pressure[32,33] followed by helium[34,35]. With DFT-MD simulations, it has been shown that the atomic disorder present in fluid helium reduces the metallization pressure significantly[36]. We therefore analyze electronic density of states in our DFT-MD simulations of neon.

Figure 10 compares total available DOSs and thermally occupied DOSs at a density of 15.0255 $\mathrm{g\,cm^{-3}}$ and temperatures of 5×10^5 and 1×10^6 K. Results were obtained by averaging over at least 100 snapshots from equally spaced DFT-MD trajectories. The eigenvales of each snapshot were aligned at their Fermi energy. To simplify Figure 10, an additional shift is introduced to align the resulting gaps at zero.

The two occupied DOS have large peaks near -30 eV reminiscent of the atomic 2s and 2p states, followed by a gap at the Fermi energy, which is then followed by a continuous spectrum of conducting states. For both temperatures, a large fraction of electrons are excited across the gap, which plays a role in the increase of pressure seen in Figure 2 and in the increase of the compression ratio of Hugoniot curves discussed in the next section. Unlike hydrogen and helium, whose gaps close turning them into metals[34,36–38], we do not find the gap for fluid neon closes for the even most extreme conditions we have studied here.

VI. SHOCK COMPRESSION

Dynamic shock compression experiments are the preferred laboratory experiments to probe the properties of materials at high pressure and temperature. Lasers[39], magnetic fields[40], and explosives[41] have been used to generate shock waves that reached megabar pressures. Under shock compression, the initial state of a material characterized by internal energy, pressure, and volume (E_0, P_0, V_0) changes to the final state described by (E, P, V). The conservation of mass, momentum, and energy yields the Hugoniot condition[42],

$$H = (E - E_0) + \frac{1}{2}(P + P_0)(V - V_0) = 0. \qquad (1)$$

For one set of initial conditions, the shock Hugoniot

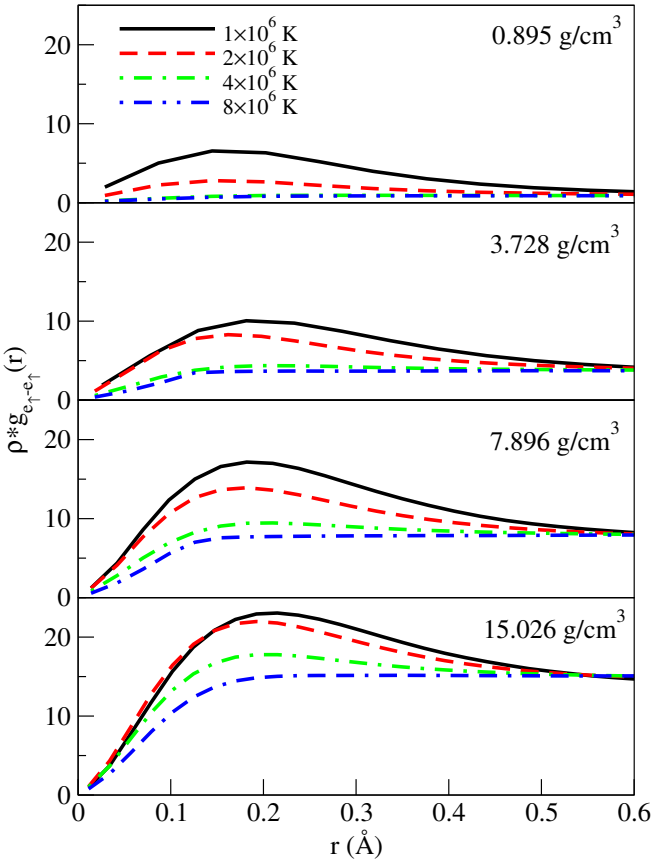

FIG. 9: (color online) The electron-electron pair-correlation functions for electrons with parallel spins calculated with PIMC.

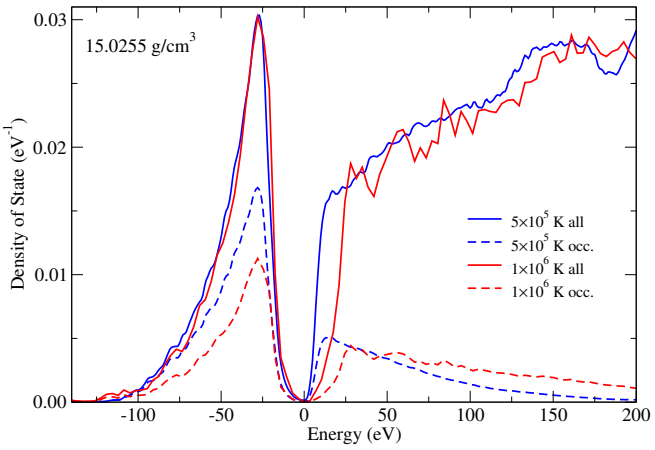

FIG. 10: (color online) Electronic density of states (DOS) of dense, fluid neon. The solid lines represent all available states while dashed lines show the occupied DOS. The curves are normalized such that the occupied DOS integrates to 1.

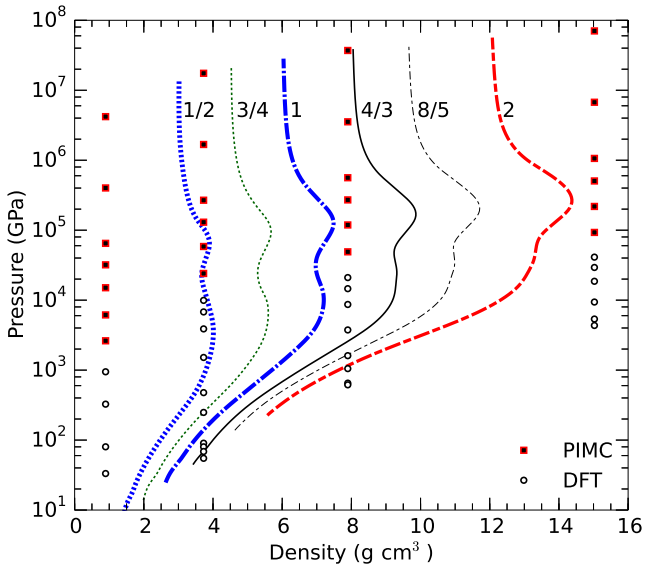

FIG. 11: (color online) Shock Hugoniot curve for different initial densities. The label on the curve specified the ratio of the initial density to that of neon at 4 K, 1.5070 g cm^{-3} .

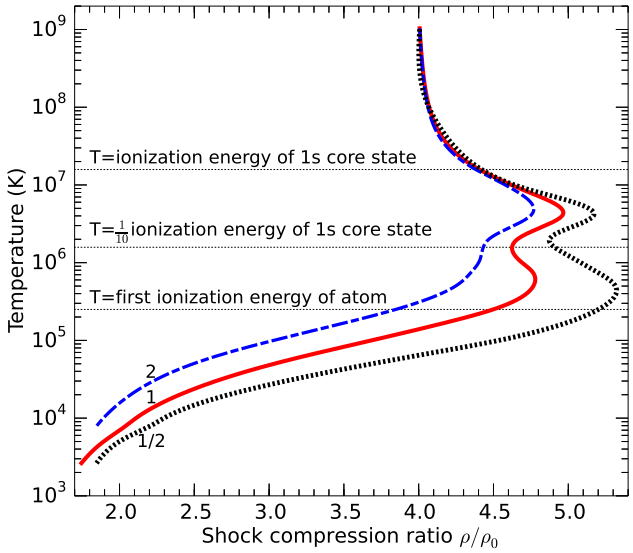

FIG. 12: (color online) Hugoniot curves for different pre-compression ratios.

curve refers to the collection of final states that can be obtained for different shock velocities. This curve can be predicted theoretically from an EOS table as given in Table I. For the initial state of the principal Hugoniot curve, we have choosen the density of solid neon at 4 K and ambient pressure, $\rho_0 = 1.5070\,\mathrm{g\,cm^{-3}}$ (Ref. [43]). We computed the corresponding internal energy with DFT calculations of a face-centered cubic (fcc) solid. The resulting Hugoniot curve has been plotted in T-P and P-ρ

spaces in Figs. 1 and 11, respectively.

Shock wave experiments have been employed diamond anvil cells to pre-compress the sample statically before a shock is launched. This technique allows one to increase the initial density and then reach much higher final densities. Thus density-temperature conditions much deeper in the interiors of planets can be reached[44]. We repeated our Hugoniot calculations for initial densities ranging from 1/2 to 2-fold the ambient value, ρ_0. P_0 and E_0 were again derived from DFT calculations of an fcc solid since experimental[45–47] and theoretical[48] work consistently predict this crystal structure for solid neon.

Figure 11 shows the resulting family of Hugoniot curves. While starting from the ambient density had led to a maximal shock density of 7.202 $\mathrm{g\,cm^{-3}}$, a 2-fold pre-compression to 13.6 GPa yields a much higher maximum shock density of 14.37 $\mathrm{g\,cm^{-3}}$, as expected. The shock compression behavior can best be analyzed by dividing the shock density by the initial density, which has been done for three representative Hugoniot curves in Figure 12. In the high-temperature limit, all curves converge to compression ratio of 4, which is the value of an ideal gas. However, compression ratios close to 4-fold may already be obtained at lower temperature where interaction effects are still important. In general, the shock compression ratio is controlled by the excitation of internal degrees of freedom that increase the compression and by interaction effects between particle that reduce it[49]. Consistent with our results for hydrogen and helium[11], we find that an increase in the initial density leads to a slight reduction in the shock compression ratio (Figure 12) because particles interact more strongly at higher density.

The Hugoniot curves in Figure 12 also exhibit two maxima if the shock densities are compared for different temperatures. The two compression maximum can be attributed to the ionization of electrons in the first and second shell. On the principal Hugoniot curve, the first maximum of ρ/ρ_0=4.779 occurs at temperature of 6.265×10^5 K (53.93 eV), which is above the first ionization energy of the neon atom, 21.56 eV. A second compression maximum of ρ/ρ_0=4.968 is found for a temperature of 4.355×10^6 K (375.3 eV). This maximum can be attributed to the ionization of the 1s core states of the neon ions. From comparison, the ionization of the last electron requires an energy of 1360 eV. In the temperature interval near the compression maximum, $2-8 \times 10^6$ K, we find a substantial reduction of the charge density around the nuclei, which we plotted in Figure 6 confirming our ionization hypothesis.

Conditions where the 1s state are partially or fully ionized are very difficult to study with DFT-MD simulations because one typically employs pseudopotential with a frozen 1s core to reach a level of efficiency that makes MD simulations with many particles possible in the first place. Thus neon is the second material after helium[49] where it has been shown that PIMC simulations are necessary to determine the maximum compression along the principle Hugoniot curve.

VII. CONCLUSIONS

In this work, we have combined PIMC with DFT-MD to construct a coherent EOS for neon for large range of densities and temperaures. The two methods validate each other near temperatures of 1×10^6 K, where both methods are capable of producing results. This work presses the limits of our combined PIMC/DMF-MD approach to computing EOSs for WDM from first-principles, where we employ only free-particle nodes in PIMC.

Unlike hydrogen and helium, we do not find neon becomes metallic for the most extreme conditions studied here.

Our analysis of the pair correlation functions describes how the structure of the plasma changes with temperature and density as atom are ionized and electrons in the first and second shells become free. The ionization imprints an signature on the shock Hugoniot curves. We find that PIMC simulations are necessary to determine the state of the highest shock compression.

Acknowledgments

This research is supported by the U. S. Department of Energy grant DE-SC0010517. Computational resources were provided in part by National Center for Atmospheric Research.

* Electronic address: kdriver@berkeley.edu; URL: http://militzer.berkeley.edu/~driver/

[1] M. Koenig *et al.*, Plasma Phys. Contr. F. **47** (2005).
[2] M. K. Matzen, Phys. Plasmas **12**, 055503 (2005).
[3] I. Cook, Nat. Mater. **5**, 77 (2006).
[4] R. Cauble, D. K. Bradley, P. M. Celliers, G. W. Collins, L. B. D. Siliva, and S. J. Moon, Contrib. Plasma Physics **41**, 239 (2001).
[5] H. M. V. Horn, Science **252**, 384 (1991).
[6] G. Chabrier, F. Douchin, and A. Y. Potekhin, J. Phys.: Condens. Matter **14**, 9133 (2002).
[7] J. J. Fortney, S. H. Glenzer, M. Koenig, B. Militzer, D. Saumon, and D. Valencia, Phys. Plasmas **16**, 041003 (2009).
[8] J. M. Lattimer, Ann. Rev. Nucl. Part. Sci. **31**, 337 (1984).
[9] J. M. Dawson, Rev. Mod. Phys. **55**, 403 (1983).
[10] F. R. Graziani, V. S. Batista, L. X. Benedict, J. I. Castor, H. Chen, S. N. Chen, C. A. Fichtl, J. N. Glosli, P. E.

Grabowski, A. T. Graf, et al., High Energy Density Physics **8**, 105 (2012).
[11] B. Militzer, Phys. Rev. B **79**, 155105 (2009).
[12] K. P. Driver and B. Militzer, Phys. Rev. Lett. **108**, 115502 (2012).
[13] B. Militzer and D. M. Ceperley, Phys. Rev. E **63**, 066404 (2001).
[14] H. F. Wilson and B. Militzer, Phys. Rev. Lett. **104**, 121101 (2010).
[15] C. L. Chen, Phys. Rev. **135** (1964).
[16] R. Cauble, M. Blaha, and J. Davis, Phys. Rev. A **29**, 3280 (1984).
[17] J. Hughto, A. S. Schneider, and C. J. Horowitz, Phys. Rev. E **82**, 066401 (2010).
[18] D. M. Ceperley, Rev. Mod. Phys. **67**, 279 (1995).
[19] J. S. Tse, Annu. Rev. Phys. Chem. **53**, 249 (2002).
[20] G. E. Jabbour and P. A. Deymier, Modelling Simul. Mater. Sci. Eng. **2**, 1111 (1994).
[21] D. M. Ceperley and B. J. Alder, Phys. Rev. Lett. **45**, 566 (1980).
[22] E. W. Brown, B. K. Clark, J. L. DuBois, and D. M. Ceperley, Phys. Rev. Lett. **110**, 146405 (2013).
[23] D. N. Mermin, Phys. Rev. **137**, A1441 (1965).
[24] F. Lambert and J. Clérouin and S. Mazevet, Europhys. Lett. **75**, 681 (2006).
[25] G. Kresse and J. Furthmüller, Phys. Rev. B **54**, 11169 (1996).
[26] P. E. Blöchl, Phys. Rev. B **50**, 17953 (1994).
[27] J. P. Perdew, K. Burke, and M. Ernzerhof, Phys. Rev. Lett. **77**, 3865 (1996).
[28] P. Debye and E. Huckel, Phys. Z. **24**, 185 (1923).
[29] For OPIUM pseudopotential generation programs, see http://opium.sourceforge.net.
[30] B. Militzer, J. Phys. A: Math. Theor. **42**, 214001 (2009).
[31] Y.-X. Yu and J. Wu, J. Chem. Phys. **117**, 10156 (2002).
[32] J. C. Boettger, Phys. Rev. B **33**, 6788 (1986).
[33] N. D. Drummond and R. J. Needs, Phys. Rev. B **73**, 024107 (2006).
[34] S. A. Khairallah and B. Militzer, Phys. Rev. Lett. **101**, 106407 (2008).
[35] B. Monserrat, N. D. Drummond, C. J. Pickard, and R. J. Needs, Phys. Rev. Lett. **112**, 055504 (2014).
[36] L. Stixrude and R. Jeanloz, Proc. Nat. Ac. Sci. **105**, 11071 (2008).
[37] P. Loubeyre, F. Occelli, and R. LeToullec, Nature **416**, 613 (2002).
[38] R. E. Cohen, I. Naumov, and R. J. Hemley, Proc. Natl. Acad. Sci. USA **110**, 13757 (2013).
[39] J. Eggert, S. Brygoo, P. Loubeyre, R. S. McWilliams, P. M. Celliers, D. G. Hicks, T. R. Boehly, R. Jeanloz, and G. W. Collins, Phys. Rev. Lett. **100**, 124503 (2008).
[40] M. D. Knudson, D. L. Hanson, J. E. Bailey, C. A. Hall, and J. R. Asay, Phys. Rev. Lett. **90**, 035505 (2003).
[41] V. E. Fortov, R. I. Ilkaev, V. A. Arinin, V. V. Burtzev, V. A. Golubev, I. L. Iosilevskiy, V. V. Khrustalev, A. L. Mikhailov, M. A. Mochalov, V. Y. Ternovoi, et al., Phys. Rev. Lett. **99**, 185001 (2007).
[42] Y. B. Zeldovich and Y. P. Raizer, *Elements of Gasdynamics and the Classical Theory of Shock Waves* (Academic Press, New York, 1968).
[43] D. N. Batchelder, D. L. Losee, and R. O. Simmons, Phys Reb. B **162**, 767 (1967).
[44] B. Militzer and W. B. Hubbard, AIP Conf. Proc. **955**, 1395 (2007).
[45] R. J. Hemley, C. S. Zha, A. P. Jephcoat, H. K. Mao, L. W. Finger, and D. E. Cox, Phys. Rev. B **39**, 11820 (1989).
[46] A. Dewaele, F. Datchi, P. Loubeyre, and M. Mezouar, Phys. Rev. B **77**, 094106 (2008).
[47] K. Takemura, T. Watanuki, K. Ohwada, A. Machida, A. Ohmura, and K. Aoki, Journal of Physics: Conference Series **215**, 012017 (2010).
[48] Y. g. He and X. z. Tang Y.-k. Pu, Physica B **405**, 4335 (2010).
[49] B. Militzer, Phys. Rev. Lett. **97**, 175501 (2006).